Theory and experiment on electromagnetic-wave-propagation velocities in stacked superconducting tunnel structures

Sakai, S.; Ustinov, A. V.; Kohlstedt, H.; Petraglia, Antonio; Pedersen, Niels Falsig

Published in:
Physical Review B Condensed Matter

Link to article, DOI:
10.1103/PhysRevB.50.12905

Publication date:
1994

Document Version
Publisher's PDF, also known as Version of record

Theory and experiment on electromagnetic-wave-propagation velocities in stacked superconducting tunnel structures

S. Sakai
Electrotechnical Laboratory, 1-1-4, Umezono, Tsukuba-shi, Ibaraki 305, Japan

A. V. Ustinov and H. Kohlstedt
Institut für Schicht- und Ionentechnik, Forschungszentrum, D-52425 Jülich, Germany

A. Petraglia and N. F. Pedersen
Physics Department, The Technical University of Denmark, DK-2800, Lyngby, Denmark
(Received 20 April 1994)

Characteristic velocities of the electromagnetic waves propagating in vertically stacked Josephson transmission are theoretically discussed. An equation for solving n velocities of the waves in an n Josephson-junction stack is derived. The solutions of two- and threefold stacks are especially focused on. Furthermore, under the assumption that all parameters of the layers are equal, analytic solutions for a generic N-fold stack are presented. The velocities of the waves in two- and three-junction stacks by Nb-Al-AlO_x-Nb systems are experimentally obtained by measuring the cavity resonance (Fiske step) modes. Comparison of the theory with the experimental data reveals good quantitative agreement.

I. INTRODUCTION

Recently, Sakai, Bodin, and Pedersen (SBP) have theoretically investigated the fluxon dynamics in superconductor-(insulator-superconductor)$_n$ multilayers.[1] Such structures can be made, for example, using Nb-(Al/AlO_x-Nb)$_n$ or NbN-(MgO_x-NbN)$_n$ Josephson tunnel junctions. Here n is the number of tunnel barriers in the multilayer. Major interest is in a very-strong-coupling case, i.e., the superconducting layer thicknesses in the inside layer are smaller than the London penetration length, where Josephson vortex currents extend over many layers. Fundamental study on various interactions of fluxon modes and small phase variation modes among different layers will give rise to a new field of the nonlinear physics and applications. One of directions for a future high-frequency application is to study phase-lock motion of fluxons.[1,2] Such a phase-locking behavior has been recently reported for Nb-(Al/AlO_x-Nb)$_2$ stacks.[3]

The SBP theory covers a variety of the system of vertically stacked Josephson junctions. In the thick limit of superconducting layers, the theory represents a series connection of single junctions. By taking the limit of zero-thickness superconducting layers (i.e., ideal two-dimensional layers) and ignoring the time-dependent terms, the formulations[4] derived from the SBP theory coincides with a vortex lattice theory[5] for strongly anisotropic high-T_c cuprate superconductors. In the limit of zero-thickness insulating layers, the SBP theory also covers the results of Volkov,[6] where the thicknesses of insulating tunnel barriers are assumed to be zero, and thus the magnetic flux penetrations in the insulating layers are neglected.

Recently Nb-(Al/AlO_x-Nb)$_n$ stacked containing up to $n=10$ have been successfully made with good fabrication controllability,[7] and Ustinov *et al.*[8] have found experimentally flux-flow and Fiske-step modes for the case of $n=2,3$. Their data revealed unique behavior of characteristic velocities that are dependent of the strong coupling in adjacent layers. A strong anisotropic cuprate superconductor, $Bi_2Sr_2CaCu_2O_x$, can be interpreted as a natural superlattice of extremely strongly coupled stacked Josephson junctions as has been discussed much in Ref. 9. The SBP theory and the analysis of the present paper are thus very useful for describing fluxon dynamics in high-temperature cuprate superconductors.

In the present paper, Sec. II describes the formulas of the electromagnetic modes and characteristic velocities on the nontunneling limit and small phase variation conditions for a general N-stacked junctions. Furthermore, the specific analytic form of two-junction and three-junction stacks are presented. A generic N-fold stack of identical junctions and layers is also discussed. Section III presents experimental results on Nb-(Al/AlO_x-Nb)$_n$ ($n=1-3$) and discusses the coupling behavior of two- and three-junction stacks as a function of the thickness of the intermediate superconducting layers. In Sec. IV, the theoretical results are compared with the experimental ones.

II. THEORY

A. Formalism

The formalism of describing the motion of fluxons in vertically stacked Josephson junctions was presented very generally in Ref. 1. In particular, the equation of motion of the overlap-type N-stacked junction (Fig. 1) is

0163-1829/94/50(17)/12905(10)/$06.00

$$\frac{\hbar}{2e\mu_0}\partial_{xx}\begin{bmatrix}\phi_{1,0}\\ \vdots\\ \vdots\\ \phi_{i,i-1}\\ \vdots\\ \vdots\\ \phi_{N,N-1}\end{bmatrix}=\begin{bmatrix} d'_{1,0} & s_1 & & & & & \\ s_1 & d'_{2,1} & s_2 & & 0 & & \\ & \ddots & \ddots & \ddots & & & \\ & & s_{i-1} & d'_{i,i-1} & s_i & & \\ & & & \ddots & \ddots & \ddots & \\ & 0 & & & \ddots & \ddots & s_{N-1} \\ & & & & & s_{N-1} & d'_{N,N-1}\end{bmatrix}\begin{bmatrix}\Delta J^Z_{1,0}\\ \vdots\\ \vdots\\ \Delta J^Z_{i,i-1}\\ \vdots\\ \vdots\\ \Delta J^Z_{N,N-1}\end{bmatrix}, \tag{1}$$

where

$$\Delta J^Z_{i,i-1}=J^Z_{i,i-1}-I_B\ , \tag{2a}$$

$$J^Z_{i,i-1}\equiv\frac{\hbar}{2e}C_{i,i-1}\partial_{tt}\phi_{i,i-1}+\frac{\hbar}{2e}G_{i,i-1}\partial_t\phi_{i,i-1}+J_{i,i-1}\sin\phi_{i,i-1}\ , \tag{2b}$$

and

$$d'_{i,i-1}=d_{i,i-1}+\lambda_{i-1}\coth\left[\frac{t_{i-1}}{\lambda_{i-1}}\right]+\lambda_i\coth\left[\frac{t_i}{\lambda_i}\right]\ , \tag{3a}$$

$$s_i=-\frac{\lambda_i}{\sinh(t_i/\lambda_i)}\ . \tag{3b}$$

Here $J^Z_{i,i-1}$ is the total current flowing in the ith junction, and I_B is the uniform bias current per unit length, which is supplied to the Nth S layer and extracted from the zeroth S layer. If there are no x-dependent excitations in the system, Eq. (1) gives $\Delta J^Z_{i,i-1}=0$ for all i. That is to say, $J^Z_{i,i-1}=I_B$ at any points at any junctions is satisfied. Thus, $\Delta J^Z_{i,i-1}$ is the total current flowing in the ith junction measured from the medium biased constantly and uniformly by I_B. $d'_{i,i-1}$ may be called the effective thickness of the junction that includes the shield current effect for the magnetic flux density in the ith insulating layer, and s_i which expresses the shield current effect of the magnetic flux density in the adjacent insulating layer, may be called the coupling parameter. To simplify the matrix expression in Eq. (1) we have defined $s_i<0$. $d_{i,i-1}$ is the barrier thickness of the ith junction, λ_i is the magnetic penetration length of the ith superconducting layer, and $C_{i,i-1}$ and $G_{i,i-1}$ are the capacitance and quasiparticle tunnel conductance, respectively, per unit length. $J_{i,i-1}$ is the dc maximum Josephson current.

If the magnetic flux density B_a is applied in parallel to the y direction of Fig. 1, the boundary conditions to be satisfied are, at both $x=0$ and $x=L$,

$$-\frac{\hbar}{2e}\partial_x\phi_{i,i-1}=B_a(s_{i-1}+d'_{i,i-1}+s_i)\qquad \text{for } i=1,2,\ldots,N\ . \tag{4}$$

B. Motion in the limit of nontunneling

Let us first consider the electromagnetic modes when both the Josephson- and quasiparticle-tunneling effects are ignored. The velocity of the electromagnetic waves that will be obtained is referred to hereafter as the *characteristic* velocity of the N junction stack. After putting zero into $G_{i,i-1}$, $J_{i,i-1}$, and I_B in Eqs. (1) and (2), the equations of motion become linear. By putting a set of exponential-type traveling waves ($j^2=-1$),

$$\phi_{i,i-1}=A_{i,i-1}\exp[jk(x-ut)]\quad \text{for } i=1,2,\ldots,N \tag{5}$$

into these linear equations, it is found that the following determinant must be zero:

$$\begin{vmatrix} \mu_0 d'_{1,0}C_{1,0}-u^{-2} & \mu_0 s_1 C_{2,1} & & & & \\ \mu_0 s_1 C_{1,0} & \mu_0 d'_{2,1}C_{2,1}-u^{-2} & \mu_0 s_2 C_{3,2} & & 0 & \\ & \mu_0 s_2 C_{2,1} & \ddots & \ddots & & \\ & & \ddots & \ddots & \ddots & \\ & 0 & & \ddots & \ddots & \mu_0 s_{N-1}C_{N,N-1} \\ & & & & \mu_0 s_{N-1}C_{N-1,N-2} & \mu_0 d'_{N,N-1}C_{N,N-1}-u^{-2}\end{vmatrix}=0\ . \tag{6}$$

The roots of this equation are the characteristic velocity of the waves of the system. In the case of noninteractions ($s_i=0$ for all i), each junction has the velocity of $|u|=(\mu_0 d'_{i,i-1}C_{i,i-1})^{-1/2}$, which is known as the Swihart velocity in a single junction.[10] In this case the stacked junctions are simply the gathering of independent single junctions. With $s_i\neq 0$ the interaction appears and these velocities are modified and solved from Eq. (6).

C. Small phase variation limit

Let us next consider a small phase variation limit under the condition of no loss ($\alpha=0$) and no bias ($\eta=0$). Then Eqs. (1) and (2) are linearized using the approximation, $\sin\phi_{i,i-1}=\phi_{i,i-1}$ for all i. The wave form

$$\phi_{i,i-1}=A_{i,i-1}\exp[j(kx-\omega t)] \tag{7}$$

can be a solution, when the dispersion relation of k vs ω satisfies the following equation:

$$\begin{vmatrix} d'_{1,0}W_{1,0}-k^2 & s_1W_{2,1} & & & \\ s_1W_{1,0} & d'_{2,1}W_{2,1}-k^2 & s_2W_{3,2} & & 0 \\ & s_2W_{2,1} & \ddots & \ddots & \\ & & \ddots & \ddots & \ddots \\ & 0 & & \ddots & \ddots \quad s_{N-1}W_{N,N-1} \\ & & & s_{N-1}W_{N-1,N-2} & d'_{N,N-1}W_{N,N-1}-k^2 \end{vmatrix}=0\ , \tag{8}$$

where

$$W_{i,i-1}=\mu C_{i,i-1}\omega^2-\frac{2e\mu_0 J_{i,i-1}}{\hbar}\ . \tag{9}$$

D. Two-junction stack

The two-junction stack ($N=2$) is not only a good example of the above-mentioned theory but also the experimentally most achievable case. Analytic forms of the characteristic velocities are easily and very generally obtained from Eq. (6). In order to investigate essential points, we consider a symmetric case that is also not far from experimental situations as discussed later. That is to say, the system has the mirror symmetry with respect to a plane cutting the middle superconducting layer equally into two, by which we have $C_{1,0}=C_{2,1}$, $G_{1,0}=G_{2,1}$, $J_{1,0}=J_{2,1}$, $t_0=t_2$, $d_{1,0}=d_{2,1}$, and $\lambda_0=\lambda_2$. Further, we have $d'_{1,0}=d'_{2,1}$, by taking Eq. (3a) into account. Then the equations of motion are

$$\partial_{xx}\begin{bmatrix}\phi_{1,0}\\ \phi_{2,1}\end{bmatrix}=\begin{bmatrix}1 & S\\ S & 1\end{bmatrix}\begin{bmatrix}\partial_{tt}\phi_{1,0}+\alpha\partial_t\phi_{1,0}+\sin\phi_{1,0}-\eta\\ \partial_{tt}\phi_{2,1}+\alpha\partial_t\phi_{2,1}+\sin\phi_{2,1}-\eta\end{bmatrix}\ . \tag{10a}$$

Another representation is

$$\begin{aligned}\frac{1}{1-S^2}\partial_{xx}\phi_{1,0}-\partial_{tt}\phi_{1,0}&=\alpha\partial_t\phi_{1,0}+\sin\phi_{1,0}\\ &\quad -\eta+\frac{S}{1-S^2}\partial_{xx}\phi_{2,1},\\ \frac{1}{1-S^2}\partial_{xx}\phi_{2,1}-\partial_{tt}\phi_{2,1}&=\alpha\partial_t\phi_{2,1}+\sin\phi_{2,1}\\ &\quad -\eta+\frac{S}{1-S^2}\partial_{xx}\phi_{1,0}\ ,\end{aligned} \tag{10b}$$

where S is the normalized coupling constant,

$$S=\frac{s_1}{d'_{1,0}}\ . \tag{11}$$

Note that $S<0$ because of the definition of s_1. In Eqs. (10), the units are also normalized: x is normalized to $\lambda_J^{(1)}$, which is the Josephson penetration length of a single junction having $d'_{1,0}$ and $J_{1,0}$. The time t is normalized to the inverse plasma angular frequency ω_0^{-1}:

$$\lambda_J^{(1)}=\left[\frac{\hbar}{2e\mu_0 d'_{1,0}J_{1,0}}\right]^{1/2}, \tag{12a}$$

$$\omega_0^{-1}=\left[\frac{\hbar C_{1,0}}{2eJ_{1,0}}\right]^{1/2}\ . \tag{12b}$$

α and η are the normalized conductance due to the quasiparticle loss and the normalized bias current, respectively, which are defined by $\alpha=G_{1,0}(\hbar/2eJ_{1,0}C_{1,0})^{1/2}$ and $\eta=I_B/J_{1,0}$.

If x is normalized to $\lambda_J^{(1)}/\sqrt{1-S^2}$ instead of $\lambda_J^{(1)}$, then $1-S^2$, appearing in both left- and right-hand sides of Eq. (10b), should be the unity, but note that, in such a case, the normalization length is no longer equal to the Josephson penetration length $\lambda_J^{(1)}$. In the limit of weak couplings ($|S|\ll 1$), $1-S^2$ in Eq. (10b) can be the unity.

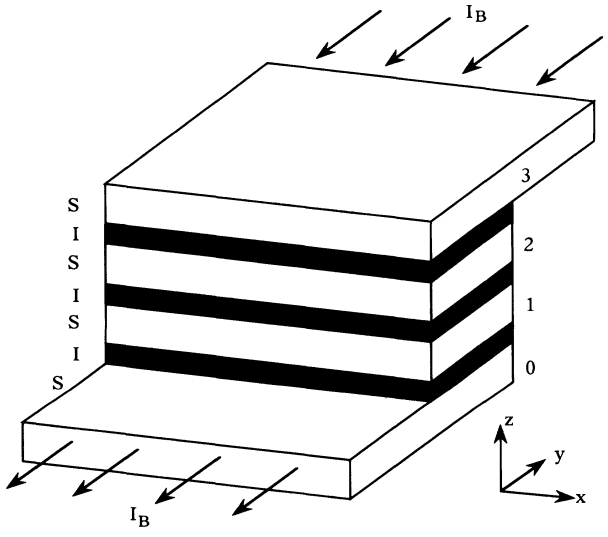

FIG. 1. A sketch of an N-fold Josephson junction stack for $N=3$.

The characteristic velocities obtained from Eq. (6) are

$$|u|=c_{\pm}\equiv c_0\frac{1}{\sqrt{1\pm S}} \tag{13a}$$

with

$$c_0=(\mu_0 d'_{1,0}C_{1,0})^{-1/2}\ , \tag{13b}$$

and the coefficients of the wave in Eq. (5) are

$$A_{1,0}=A_{2,1}\ \text{ for }|u|=c_+\ , \tag{14a}$$

$$A_{1,0}=-A_{2,1}\ \text{ for }|u|=c_-\ . \tag{14b}$$

Thus, in the case of $|u|=c_+$, the phases change in an in-phase manner, and, in the case of $|u|=c_-$, they change in an out-of-phase manner.

The plasma dispersion relation described in Sec. II C is, in this two-junction stack case, expressed as

$$\omega^2=\frac{k^2}{1\pm S}+1\ . \tag{15}$$

At the limit of $k\rightarrow\infty$, u $(=\omega/k)$ approaches asymptotically the characteristic velocity $c_{\pm}$ in Eq. (12). As shown in Ref. 1, in the bunched coherent mode of the soliton in the two-junction stack, the velocity approaches c_+, and the separate symmetric mode (when the fluxons move separately) approaches c_-. From these discussions the characteristic velocities obtained in the limit of nontunneling are essential quantities describing the electromagnetic-wave propagation such as fluxons and small phase varying modes in the system.

E. Three-junction stack

Here we discuss the characteristic velocities in the limit of nontunneling. From Eq. (6) we can obtain analytic form, but to avoid the complexity of the expression, we assume a similar symmetric configuration to the one we have discussed in the case of the two-junction stack. That is, the system is mirror symmetric with respect to the plane cutting the middle insulating layer equally into two. Thus, we have $t_0=t_3$, $t_1=t_2$, $\lambda_0=\lambda_3$, $\lambda_1=\lambda_2$, $d_{1,0}=d_{3,2}$, $C_{1,0}=C_{3,2}$, $G_{1,0}=G_{3,2}$, and $J_{1,0}=J_{3,2}$. These give automatically $s_1=s_2$ and $d'_{1,0}=d'_{3,2}$. In addition, we assume the capacitance in the middle junction is equal to the others, i.e., $C_{2,1}=C_{1,0}$. Then we have three characteristic velocities u_-, u_m, and u_+:

$$u_m=(\mu_0 d'_{1,0}C_{1,0})^{-1/2}\ , \tag{16a}$$

$$u_{\pm}=\sqrt{2}u_m\left\{1+\frac{d'_{2,1}}{d'_{1,0}}\mp\left[\left[1-\frac{d'_{2,1}}{d'_{1,0}}\right]^2+8\left[\frac{s_1}{d'_{1,0}}\right]^2\right]^{1/2}\right\}^{-1/2}\ . \tag{16b}$$

Note that the relation $u_-<u_m<u_+$ is always correct and, needless to say, we have the velocities of the same values and opposite polarity $(u<0)$. The coefficients of the wave form in Eq. (5) are for $u=u_m$.

$$A_{1,0}=-A_{3,2}, A_{2,1}=0\ , \tag{17a}$$

and for $u=u_{\pm}$,

$$A_{1,0}=A_{3,2}\ ,$$

$$A_{2,1}=-\frac{A_{1,0}d'_{1,0}}{2s_1}\left\{1-\frac{d'_{2,1}}{d'_{1,0}}\pm\left[\left[1-\frac{d'_{2,1}}{d'_{1,0}}\right]^2+8\left[\frac{s_1}{d'_{1,0}}\right]^2\right]^{1/2}\right\}\ . \tag{17b}$$

In the mode of $u=u_m$, the phase in the bottom junction changes in the out-of-phase manner with respect to the phase in the top junction. For the mode of the highest velocity $(u=u_+)$, the phases of three junctions varies in an in-phase manner. (Note that $s_1<0$.) For the mode of the lowest velocity $(u=u_-)$, only the phase in the middle junction varies in an out-of-phase manner with respect to the other junction phases.

F. An *N*-fold stack of identical junctions and layers

Let us consider a generic N-fold stack, where all superconducting layers are identical and the insulating layers are identical. One of possible cases is a $Bi_2Sr_2CaCu_2O_x$ single crystal, which may be regarded as a natural superlattice.[9] In this case, all subscripts in $d'_{i,i-1}$, s_i, $C_{i,i-1}$, $J_{i,i-1}$, and $W_{i,i-1}$ (for $i=1,2,\ldots,N$) can be eliminated, and thus the determinants in Eqs. (6) and (8) for the characteristic velocities and the dispersion relation, respectively, have a well-known tridiagonal symmetric form.[11] Consequently, the analytic forms of the eigenvalues of Eqs. (6) and (8) are given by

$$c_n^{(N)}=\left\{\frac{1}{1+2S\cos[n\pi/(N+1)]}\right\}^{1/2}\quad\text{for } n=1,2,\ldots,N \tag{18}$$

and

$$[\omega_n^{(N)}]^2=1+\frac{k^2}{1+2S\cos[n\pi/(N+1)]}\quad\text{for } n=1,2,\ldots,N\ . \tag{19}$$

Here the normalization used with respect to S, x, and t is similar to that in Sec. II D [Eqs. (11) and (12)]. The only differences are that all the subscripts in Eqs. (11) and (12) are eliminated by the assumption of identical junctions and layers. Thus, k and $\omega_n^{(N)}$ are normalized to the inverse Josephson penetration length $\lambda_J^{(1)}$ and the plasma angular frequency ω_0, respectively, and $c_n^{(N)}$ is normalized to $\lambda_J^{(1)}\omega_0$.

The dynamics is given by the eigenvectors

$$A^n_{i,i-1}=\left[\frac{2}{N+1}\right]^{1/2}\sin\left[\frac{in\pi}{N+1}\right]\quad\text{for } n=1,2,\ldots,N \text{ and } i=1,2,\ldots,N\ , \tag{20}$$

where the index n corresponds to different velocities and i represents the ith layer. From these relations we make the following observations: (1) The dynamics does not

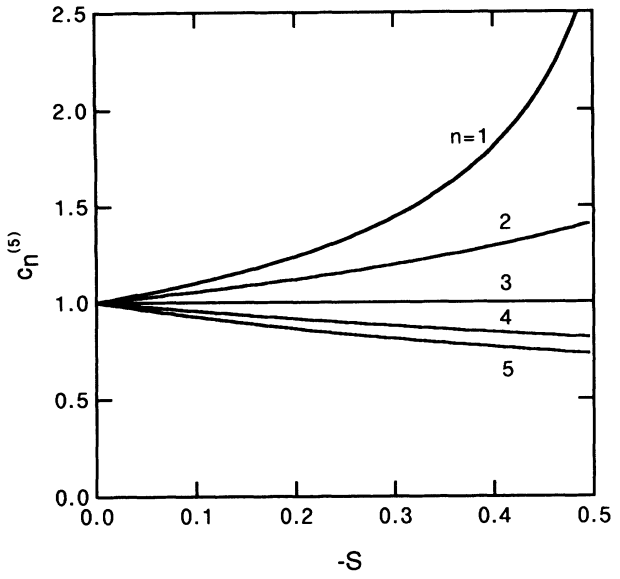

FIG. 2. The characteristic velocities in a fivefold stack of identical junctions as a function of the coupling parameter S.

depend on the coupling factor S, which is a characteristic of all the identical junction. It generally depends on S as shown in Eq. (17b). (2) For an N-layer stacked junction we have N different limit velocities. (3) The index n determines the state of all junctions. All variables, $\omega_n^{(N)}, c_n^{(N)}$ for different junctions in a definite state are the same. (4) For $n=1$, i.e., the largest velocity, all the amplitudes have the same sign (the arguments of sine are always in the first and second quadrants), which means an in-phase behavior. (5) For $n=N$, the smallest velocity, neighboring amplitudes are always opposite, indeed the arguments of sine now stay alternatively in the first (or second) quadrant and third (or fourth) quadrant. (6) The results in the case $N=2,3$ coincide perfectly with the special case (i.e., all the equal junction cases) of the results of the preceding subsections.

Note that using a different approach, units, and normalization, Eq. (19) was also obtained by Kleiner[12] for the resonant modes of a finite n-stacked junction embedded in a field different from zero. As an example of application, Fig. 2 shows the normalized velocities in a fivefold stack varying the coupling parameter.

III. EXPERIMENTAL RESULTS

In order to study the dynamics of the electromagnetic waves in the stacked junctions, we investigated resonant structure on IV characteristics in the applied magnetic field, which are known as Fiske steps[13] (FS's). In general, such resonances occur when the Josephson generation frequency coincides with the frequency of one of the cavity modes in the junction. For a junction of length L, the cavity mode frequencies correspond to an integer number n of half wavelengths on the junction length and are given by the relation

$$f_n = \frac{nc}{2L} , \tag{21}$$

where c is the electromagnetic wave propagation velocity in the junction called Swihart velocity. This is the characteristic velocity in a single junction. Because of the ac Josephson relation, each resonance [Eq. (21)] yields a step at approximately constant voltage in the IV characteristics of the junction. The external magnetic field provides a spatial modulation of the Josephson pair current in the junction and determines the current amplitudes of the steps in the IV curve. For a single barrier junction with given c and L, one observes a set of voltage-equidistant steps, which we call a "Fiske-step (FS) family," with a voltage spacing $\Delta V_{\rm FS}=\Phi_0 f_1$. In a stack of N junctions, the velocity c is predicted to have N possible different values (see Sec. II); thus, N different FS families are expected to be seen in the IV characteristics.

In a long junction placed in sufficiently high magnetic field H, the fluxon motion gives rise to a flux-flow (FF) step in the IV curve. At the flux-flow regime, fluxons perform a unidirectional motion with the velocity close to the Swihart velocity of the junction. Typically, in a junction of a finite length, a flux-flow step appears as one or two neighboring Fiske steps at the maximum of their current amplitude. Increasing the magnetic field yields the increase of the flux-flow-step voltage, and thereby the flux-flow voltage hits the FS with high numbers n.

For twofold and threefold stacks the Fiske-step splitting in different families has been observed in Ref. 8, where stacks with only one t value ($t=35$ nm) were investigated. It was noted that the difference in the voltage spacing of different FS families, $\Delta V_{{\rm FS}i}$ (index i denotes the number of the FS family), should depend on the magnetic coupling between the junctions, i.e., on the thickness t of the intermediate superconducting layers. In this section we report a quantitative investigation of the voltage spacing $\Delta V_{{\rm FS}i}$ dependence on t for twofold and threefold stacks.

A. Samples

The fabrication method for stacked Nb-(Al/AlO_x-Nb)$_n$ tunnel junctions containing up to $n=10$ tunnel barriers has been demonstrated.[7] In the present study, high-quality Nb-(Al/AlO_x-Nb)$_n$ Josephson tunnel junctions with $n=1$, 2, and 3 were fabricated. The gap voltages were about 2.6 mV and varied for the different junctions in one stack within 2–3 %. The difference between the critical current densities (of typical $J_c=200$ A/cm^2) in one stack was estimated from the maximum currents at the gap voltages and found typically to be less than 20%. The thickness t of the intermediate Nb layer between the junctions in different stacks varied from 30 to 140 nm. These values cover the thickness interval of interest, around the London penetration depth λ, which for our sputtered Nb was estimated to be 90 nm. The parameters of the samples are summarized in Table I.

A typical value for the Josephson penetration depth λ_J in our single-barrier junctions was about 25 μm. For a quasi-one-dimensional long junction, the length L and width W have to be $L \gg \lambda_J$, and $W < \lambda_J$. In the present work we used the stacks with the dimensions in plane L from 150 to 400 μm and W from 10 to 40 μm (see Table I).

TABLE I. Parameters of the investigated samples.

Sample No.	L (μm)	W (μm)	t_0 (nm)	t_1 (nm)	t_2 (nm)	t_3 (nm)	ΔV_{FS1} (μV)	ΔV_{FS2} (μV)	ΔV_{FS3} (μV)
1	150	20	90	330			50±2.0		
2	200	40	90	330			37.5±1.0		
3	300	10	90	330			26±0.4		
4	400	10	90	330			17.4±0.3		
5	300	10	90	30	330		13±0.5	30±2.5	
6	200	40	90	30	330		18.5±0.3	45.0±0.8	
7	400	20	105	140	330		15.6±1.0	19.2±1.0	
8	300	10	90	120	330		20.5±0.7	25.1±1.0	
9	300	20	70	105	330		20.4±0.3	28.2±0.5	
10	200	40	90	60	330		26±1.5	46±2.5	
11	200	20	180	90	615		27.5±0.4	38.3±0.6	
12	200	10	100	130	330		32.5±0.5	39.0±0.8	
13	150	20	100	35	35	300	21±1.0	33±2.0	78±3.0
14	400	10	90	60	60	330	10.4±0.2	16±1.0	22.7±0.6
15	200	20	180	90	90	615	26.2±0.5	31.2±0.8	50.3±1.5

During the measurements a sample was surrounded by a cryoperm shield. The magnetic field H was applied by a solenoid inside the shield in the plane of the tunnel barrier and perpendicular to the larger dimension L of the junctions. Measurements were performed at $T=4.2$ K. In the IV curves presented below, the stacked junctions are measured in series. During the field sweeps, the IV curves were preamplified and recorded by a digital storage oscilloscope.

B. IV characteristics

Typical IV characteristics of a twofold stack in the applied magnetic field is shown in Fig. 3(a). In this stack one of the junctions (A) had somewhat lower critical current than junction B. Thus, in the applied external magnetic field H, the magnetic flux was first entering junction A, and then, at the higher fields, junction B. In a finite bias current, there was an interval of H, where junction A switched to the flux-flow state, while junction B stayed at the stationary (zero-voltage) state. In Fig. 3(a), when the bias current I is increased from zero, the flux-flow step FF1 corresponding to the lowest FS family in A is traced up to $V=V_{FF1}$. At some current junction, A switches to the single junction gap voltage V_g of about 2.5 mV. The single gap voltage is observed because the other junction B is still not switched to the gap. Further increase of I leads to the switching of junction B to the second gap voltage (not shown). If from the state at the first gap voltage the current is decreased, with B not yet switched, we observe another flux-flow step (FF2) corresponding to the second FS family (at $V=V_{FF2}$) in junction A. Both voltages V_{FF1} and V_{FF2} were found to increase approximately linearly with H. Each flux-flow step (FF1 and FF2) consists of a series of Fiske steps (FS1 and FS2). It is worth noting that these separate Fiske-step families appear in different voltage ranges but are observed in the same junction (A) of the stack. The single junction origin of the steps FF1 and FF2 is confirmed by appearance of very similar branches (as FF1 and FF2) between the first and the second gap, at 3.2–3.6 mV. Such

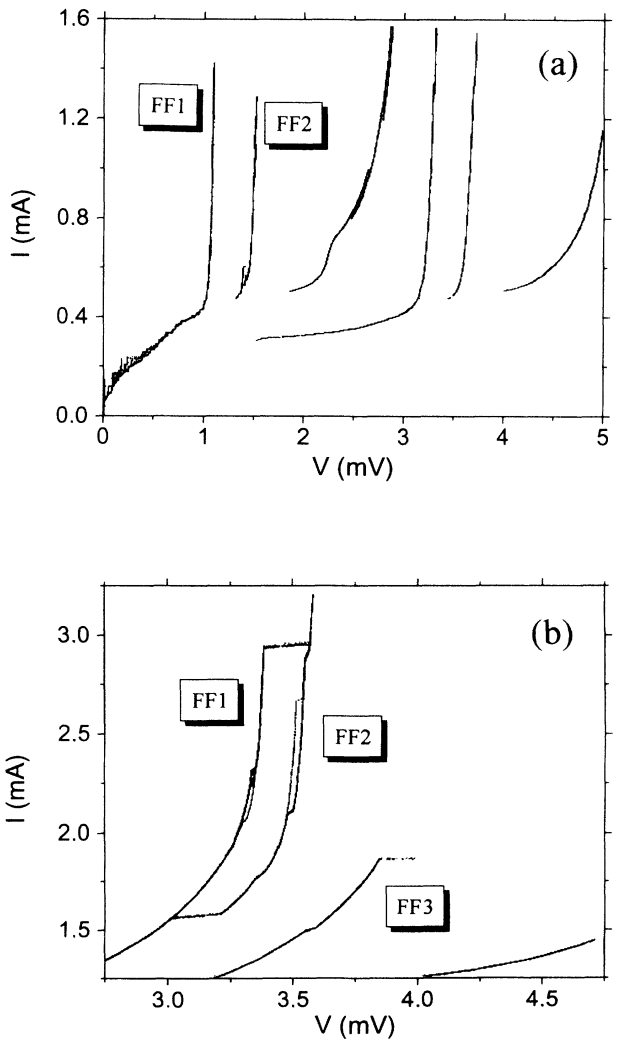

FIG. 3. Typical IV curves with flux-flow steps of twofold stack No. 8 (a) and threefold stack No. 15 (b) in the applied magnetic field.

traces [see Fig. 3(a)] were observed when the current is decreased from the bias point at the second gap ($V=2V_g$). These steps are the same branches FF1 and FF2 in junction A added to the gap voltage of junction B. The high rate of the quasiparticle injection into the common electrode by junction B at $V=V_g$ increases the losses in junction A. This makes the resonances above the first gap smoother, more stable, and even easier to measure than the lower ones. In higher magnetic field, we observed flux-flow branches similar to FF1 and FF2, but in junction B. These branches appeared in a similar manner between the first and the second gap voltages. Within the experimental error their Fiske step voltage spacings (see below) were found to be equal to those in junction A.

Carrying out similar measurements on threefold stacks, we found three flux-fold steps, as expected. Figure 3(b) shows such an example of the steps observed between the first and the second gap voltage in a threefold stack. These steps correspond to the fluxon motion in one of the junctions in the stack (one of the other two junctions remains in the stationary state, and the other one is switched to the gap state). For the weakly coupled stacks with large t, it was more difficult to distinguish between different FS families due to their close voltage ranges.

C. Measurements of the Fiske step voltage spacings

Figure 4 shows multiple traces of the IV curve of the threefold stack sample 15 [shown in Fig. 3(b)] obtained with continuously varying the external magnetic field H using a digital storage oscilloscope. Each flux-flow step [FF1, FF2, and FF3, as shown in Fig. 3(b)] consists of a series of Fiske steps (FS1, FS2, and FS3). To obtain the field tuning picture of the steps FF2 and FF3, after biasing on the step, we swept the current in small intervals and varied the field H. This procedure was necessary to avoid switching between different families of steps on the hysteretic IV curve of the stack. As seen in the insets of Fig. 4, each flux-flow step displays a different voltage spacing between the Fiske steps. Such a measuring routine has been performed for samples with different number of barriers $n=2,3$ and electrode thicknesses.

Table I summarizes measured spacings between the steps for various FS families in different stacks. In each case, the voltage spacings were measured several times between different steps and the experimental mean square error was calculated. These measurements were easier to perform for stacks with small t (strong coupling), where the voltage intervals of different FS families did not overlap, and there was a clear distinction between these families. For larger t (weaker coupling) a voltage interval of every FS family was more narrow, thus increasing the experimental error.

We note that the presented data contain additional experimental uncertainties due to the difference in the measured frequency ranges for different FS families. Some of the Fiske steps were found to be stable only in narrow voltage intervals near 1 mV or higher where the effects of dispersion already play an important role. At frequencies comparable with the gap frequency (about 650 GHz for our Nb) the phase velocity is expected to decrease. This gives a decreasing of the Fiske-step voltage spacing at high voltages, which we always observed in experiments with single-barrier Nb junctions. We did not study this effect systematically for the stacked junctions; its role is estimated to be a possible relative correction of 5–8 % for some FS families (in particular, FSF2 and FSF3).

Table I clearly shows the general tendency predicted by the theory. With decreasing t, the coupling between the junctions in a stack is expected to increase, thereby increasing the difference between c_- and c_+ (the difference Fiske-step voltage spacings of FS families). A detailed quantitative comparison of the theory with the experiment is made in the following section.

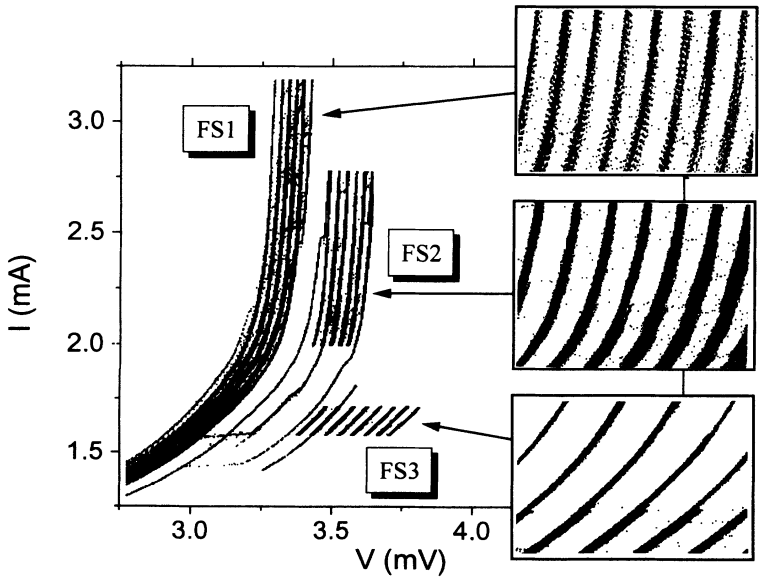

FIG. 4. Stored traces of the Fiske steps obtained by varying the external magnetic field for a stack No. 15. A single IV curve is shown in Fig. 3(b) for a fixed field value. Insets show the Fiske step structure on the expanded by factor of 4 voltage scale.

IV. COMPARISON OF THE THEORY WITH THE EXPERIMENT

Before analyzing the stacked junction data, we first discuss the characteristic (Swihart) velocity of ordinary single junctions. The velocity is obtained by $c^{(1)}=2L(\Delta V_{FS})/\Phi_0$. Using the data in Table I, the velocity is found in the range, $(6.6-7.6)\times 10^6$ m/s, with the mean value of 7.2×10^6 m/s. Since the velocity is also expressed as Eq. (13b) using the junction parameters, the specific capacitance obtained is 7.3 μF/cm^2 on the average, which is in good agreement with the data published.[14]

A. The two-junction stack

As described in the preceding section, the thickness of the top superconducting layer is different from that of the bottom superconducting layer, and these are also different from sample to sample. In the data analysis below these differences are taken into account, but the difference of the capacitance between the top and bottom junctions is ignored. The spread of the critical current density, which is very sensitive to the barrier thickness values, between both the top and bottom junctions did not exceed 30–40 % for all the samples listed in Table I. Thus, we can assume that the capacitances, which are much less sensitive to the barrier thicknesses, are identical. When the thickness difference of the superconducting layers ($t_0\neq t_2$) is considered, the expression of the characteristic velocities of Eq. (12) is modified as

$$c_{\pm}=c_0\frac{1}{\sqrt{1\pm S^*}}\ , \tag{22}$$

where c_0 is defined in Eq. (13b) and

$$S^*=\kappa S_1\ , \tag{23}$$

with

$$\kappa=\left[1+\frac{1-D'_{1,0}D'_{2,1}}{S_1^2}\right]^{1/2}. \tag{24}$$

Here κ is the correction factor due to the asymmetry coming from the thickness difference, and

$$\begin{aligned} D'_{1,0}&=d'_{1,0}/d'_{\rm av}\ ,\\ D'_{2,1}&=d'_{2,1}/d'_{\rm av}\ ,\\ S_1&=s_1/d'_{\rm av}\ ,\\ d'_{\rm av}&=(d'_{1,0}+d'_{2,1})/2\ , \end{aligned} \tag{25}$$

where $d'_{\rm av}$ is the averaged effective thickness, and $D'_{i,i-1}$ and S_1 are the effective thickness and coupling constant normalized to $d'_{\rm av}$, respectively.

The precise value of the capacitance is sensitive to fabrication technology. So we first use a good method of comparison in which the effect of capacitance does not appear explicitly. From Eq. (22), we have a relationship between the velocities and the coupling constant:

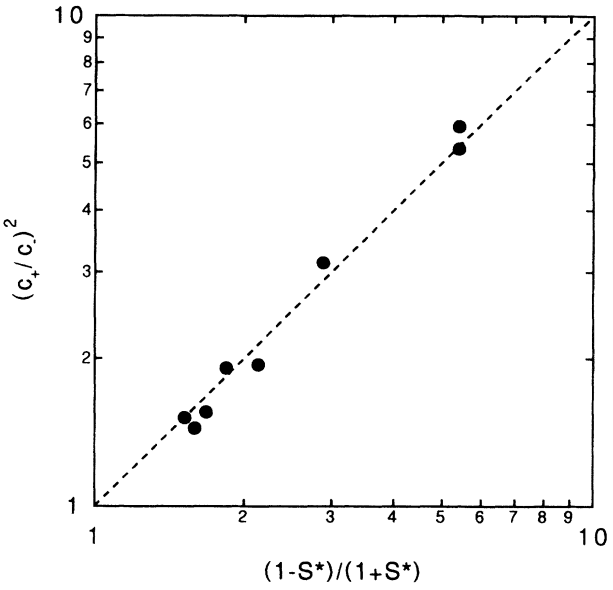

FIG. 5. Plot of experimental data for twofold stacks (points) on a plane of $(c_+/c_-)^2$ vs $(1-S^*)/(1+S^*)$. The theory predicts that these quantities are equal, as shown by the dashed line in the figure. This analysis is independent of the junction capacitance.

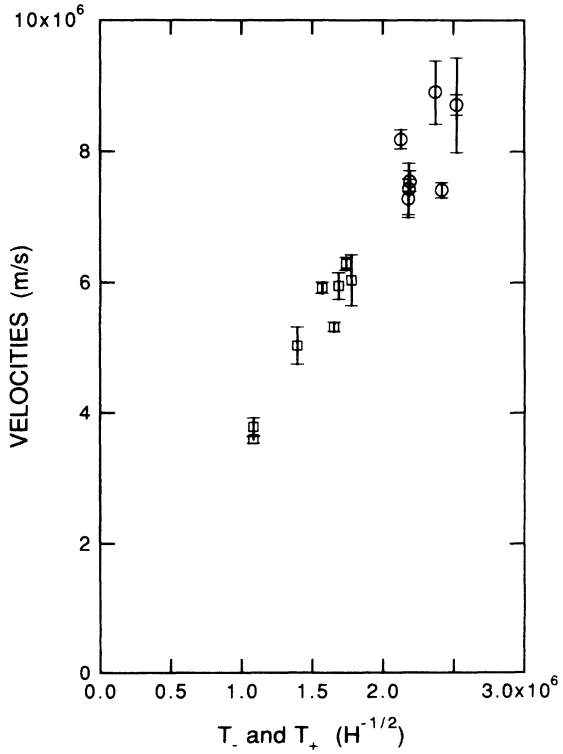

FIG. 6. Experimental data for twofold stacks as c_- vs T_- (squares) and c_+ vs T_+ (circles). A linear dependence is theoretically predicted with equal proportionality factors for c_- vs T_- and in c_+ vs T_+. The uncertainties of the measured data (listed in Table I) are given by error bars.

TABLE II. List of both the theoretical and experimental characteristic velocities for three-junction stacks.

	Theory			Experiment		
Sample No.	u_-	u_m ($\times 10^6$ m/s)	u_+	u_-	u_m ($\times 10^6$ m/s)	u_+
13	3.4	5.0	9.6	3.1±0.15	4.8±0.3	11±0.4
14	4.3	5.7	8.8	4.0±0.1	6.2±0.4	8.8±0.2
15	5.1	6.4	8.7	5.1±0.1	6.0±0.15	9.7±0.3

$$\left[\frac{c_+}{c_-}\right]^2=\frac{1-S^*}{1+S^*}\ , \tag{26}$$

where no capacitance terms are included. Using the values of the superconducting-layer thicknesses and the obtained velocities in Table I, we get, in Fig. 5, experimental relationship between the left- and right-hand sides of Eq. (26), which is in very good agreement with the theoretical dashed curve in the figure. Here we used no fitting parameters except the well-known value of 90 nm for the magnetic penetration length of λ_i ($i=0,1,2$) in all the superconducting layers. Even the ±10% change of this value does not affect this good agreement. Note that, in consequence, the asymmetric correction factor κ is very close to the unity (around the range from 1.002 to 1.04) for all samples in Table I.

Next we discuss the absolute values of the velocities. Using the Fiske-step voltage relation and the experimental data in Table I we obtain experimental values for the velocities. In the theoretical result [Eq. (22)], $d'_{1,0}$ in c_0 depends on the thickness of the samples. To eliminate this geometric effect from sample to sample, the geometric and physical parameters of each sample are gathered in $T_\pm=[\mu_0 d'_{1,0}(1\pm S^*)]^{-1/2}$, and we have

$$c_\pm=\frac{1}{\sqrt{C_{1,0}}}T_\pm\ . \tag{27}$$

Figure 6 shows the plot data of the experimentally obtained, c_+ vs T_+ (circles) and c_- vs T_- (squares). We find that the results obey the theoretical prediction, i.e., the $c_\pm$-vs-$T_\pm$ proportional relationship.

The proportional factor is only a function of the specific junction capacitance that may be sensitive to the fabrication technology. Thus the data spread in Fig. 6 is partially due to this technological reason and partially due to the uncertainty of the measurement that was shown by error bars in the figure. The lowest and highest estimations of the capacitance from the plot in this figure are 6.9 and 11 μF/cm^2, respectively.

B. The three-junction stack

Let us discuss the result of sample 13. The thickness of each superconducting layer is the following: $t_0=100$ nm, $t_1=t_2=35$ nm, and $t_3=300$ nm. Using $\lambda_i=90$ nm for all i, the relative deviation between $d_{1,0}$ and $d_{3,2}$, $|d'_{3,2}-d'_{1,0}|/d'_{1,0}$, is only 3%. The system may be regarded to have the mirror-symmetric configuration used in Sec. II E. From Table I, the experimentally obtained Fiske-step spacings are 21, 33, and 78 μV, and the corresponding velocities are 3.1×10^6, 4.8×10^6, and 11.3×10^6 m/s. Let C_{10} be equal to 9 μF/cm^2, which is the average of the specific capacitance of the two-junction stack data. By using this value for u_m and putting $t_1=t_2=35$ nm and $\lambda_i=90$ nm for all i, we obtain $u_-=3.4\times10^6$, $u_m=5.0\times10^6$, and $u_+=9.6\times10^6$ m/s, which explain the experimental values very consistently. For samples 14 and 15, the same analysis was made. The results are summarized in Table II, where the agreement between the theory and experiment is found to be good.

V. SUMMARY

Characteristic velocities governing the electromagnetic wave propagation of various modes in vertically stacked Josephson junctions are investigated here theoretically and experimentally. An equation for these velocities is derived, which indicates the existence of n velocities in an n-junction stack. The velocities obtained from resonance mode observations for two- and three-junction stacks of Nb-Al-AlO$_x$-Nb systems are compared with the theory, and good agreement is found.

ACKNOWLEDGMENTS

We would like to acknowledge useful discussions with P. Barbara, P. Bodin, M. Cirillo, R. Kleiner, and P. Müller.

[1]S. Sakai, P. Bodin, and N. F. Pedersen, J. Appl. Phys. **73**, 2411 (1993).

[2]N. Groenbech-Jensen, M. R. Samuelsen, P. S. Lomdahl, and J. A. Blackburn, Phys. Rev. **42**, 3976 (1990); N. Groenbech-Jensen and J. A. Blackburn, Phys. Rev. Lett. **70**, 1251 (1993); N. Groenbech-Jensen, D. Cai, and M. R. Samuelsen, Phys. Rev. B **48**, 16 160 (1993).

[3]A. V. Ustinov, H. Kohlstedt, and C. Heiden, in *Applied Superconductivity*, edited by H. C. Freyhardt (DGM Infomationgesellshaft Verlag, Obcrursel, 1993), Vol. 2, p. 1239.

[4]When the zero thickness limit of superconducting layers is taken, the sheet density of the pair electrons (or holes) instead of the volume density should be nonzero finite values.

[5]L. Bulaevskii and J. R. Clem, Phys. Rev. B **44**, 10 234 (1991).

[6]A. F. Volkov, Pis'ma Zh. Eksp. Teor. Fiz. **45**, 299 (1987) [JETP Lett. **45**, 376 (1987)].

[7]H. Kohlstedt, G. Hallmanns, I. P. Nevirkovets, D. Guggi, and C. Heiden, IEEE Trans. Appl. Supercond. **3**, 2197 (1993).
[8]A. V. Ustinov, M. Cirillo, N. F. Pedersen, G. Hallmanns, and C. Heiden, Phys. Rev. B **48**, 10 614 (1993).
[9]R. Kleiner and P. Müller, Phys. Rev. B **49**, 1327 (1994); R. Kleiner, P. Müller, H. Kohlstedt, N. F. Pedersen, and S. Sakai, *ibid.* **50**, 3942 (1994).
[10]J. C. Swihart, J. Appl. Phys. **32**, 461 (1961).
[11]R. Zurmuhul and S. Falk, *Matrizen* (Springer-Verlag, Berlin, 1984), Teil 1.
[12]R. Kleiner, Phys. Rev. B **50**, 6919 (1994).
[13]M. D. Fiske, Rev. Mod. Phys. **36**, 839 (1964).
[14]M. Gurvitch *et al.*, Appl. Phys. Lett. **42**, 472 (1983); S. Morohashi and S. Hasuo, J. Appl. Phys. **61**, 4835 (1987).